Spin-density contribution in the optical potential of open j-shell nuclei

Keshab C. Panda
School of Physics, Sambalpur University, Jyoti Vihar, Sambalpur 768019, India

Binod C. Sahu
Panchayat College, Bargarh 768038, India

Raj K. Gupta
Department of Physics, Panjab University, Chandigarh 160014, India

(Received 12 April 2013; revised manuscript received 19 July 2013; published 5 September 2013)

The energy-dependent real and imaginary parts of the optical potential of some twenty pairs of spin-unsaturated, open j-shell nuclei are calculated in the energy density model, using the complex Skyrme III energy density. The calculated potentials, without any renormalization, reproduce the experimental data on elastic scattering cross sections of all the pairs of nuclei studied. The contribution of the spin density terms, of the Skyrme III energy density, toward such potentials and toward the corresponding elastic scattering cross sections and sub-barrier fusion cross sections are investigated.

DOI: 10.1103/PhysRevC.88.034602 PACS number(s): 24.10.Ht, 25.70.Bc, 25.70.Jj

I. INTRODUCTION

In heavy-ion reactions, rich varieties of novel manifestations take place in the exit channel due to the strong interaction between the heavy ions. These events, characterized by the incident energy, mass, and structural properties of the colliding ions, are expected to add significantly to our present knowledge of nuclear properties. The understanding of these events requires the microscopic heavy-ion interaction potential that properly contains the effects of relative motion and structural properties of colliding nuclei. Therefore, gaining knowledge of such an interaction potential has been one of the major problems in nuclear physics.

In the recent past, initial efforts were made by Kaur and Chattopadhyay [1] and Panda [2] to illustrate the structural effects of the spin density of unsaturated, closed j-shell nuclei on the microscopic calculation of their interaction potential. Since the spin density arises from the nucleonic configuration of the last unfilled l shell of the nucleus, it is expected to play an important role in the heavy-ion reactions involving weak to strong overlap of the projectile and target densities. In the region of weak overlap, elastic scattering occurs and it is observed that the heavy-ion elastic scattering cross sections of spin-saturated nuclei are nicely described by a microscopic optical potential [3–5] that does not contain any adjustable parameter or need renormalization. The microscopic calculation of the energy-dependent real and imaginary parts of such an optical potential requires only a two-body effective interaction and the density distributions of the projectile and target nuclei as inputs. Panda and Patra [6] extended this technique to *spin-unsaturated, closed j-shell* nuclei, and they showed the structural effects of the spin densities on their potential and the corresponding elastic scattering cross sections. The real and imaginary parts of the optical potential were calculated [6] by taking (i) the Skyrme III effective interaction [7], (ii) the parametrized self-consistent matter densities [8], and (iii) the spin densities obtained from the shell-model wave functions by using the prescription of Vautherin and Brink [9] as inputs in the energy density model (EDM). The calculated optical potential also reproduced nicely the elastic scattering data of spin-unsaturated, closed j-shell nuclei, without any renormalization. However, the contribution of the spin density toward the real and imaginary potentials, in the region sensitive to elastic scattering, was not appreciable and essentially had no effect on the elastic scattering angular distributions. Also, the effects of spin density on sub-barrier fusion, which involves more overlap of the densities of spin-unsaturated, closed j-shell nuclei, were investigated by Puri and Gupta [10,11], by using the real part of the optical potential in the barrier penetration model. They found that the positions and heights of the fusion barriers and the fusion cross sections are affected within $\sim$1% only, since the closed j-shell nuclei are very weakly spin-unsaturated.

Recently, Gupta and collaborators [12–15] have also investigated the contribution of spin density on the energy-independent real part of the interaction potential of *highly spin unsaturated, open j-shell*, even-even nuclei. They have calculated the real potential by using the Skyrme II effective interaction [7], the experimental nucleonic densities of the target and projectile [16,17], and the spin density obtained from the shell-model wave functions in the proximity model approximation [18]. This calculation shows that the contribution of spin density is rather large. In the relevant region, the contribution is repulsive and reduces the energy-independent real potential by as much as 5–7 MeV at the repulsive maxima of the spin-density potential. A similar contribution toward the imaginary part of the optical potential is highly expected since, from our previous analysis [4–6], it is evident that the elastic scattering data are very much sensitive to the variation of both the real and imaginary potentials. Hence, the role of spin density of open j-shell even-even nuclei might be important in determining the elastic scattering optical potential and the corresponding elastic scattering cross section and sub-barrier fusion cross section [3,19]. This enables one to test the accuracy of the radial dependence of the same potential in different regions of nuclear reaction data and to provide new

information on the physics taking place when two nuclei come together. We investigate these aspects in the present paper.

The aim of the present paper is at least threefold: 1. to properly calculate the energy-dependent real and imaginary parts of the optical potential of those pairs of nuclei having at least one being an open j-shell nucleus, 2. to study the effect of the spin-density terms on the real and imaginary parts of the calculated energy-dependent potentials in different radial regions, and 3. to study the role of spin density on the elastic scattering and sub-barrier fusion cross sections of the chosen pairs of nuclei and to estimate the percentage contribution of the spin density in the relevant region of the potential sensitive to these nuclear reactions.

The paper is organized as follows: In Sec. II, we present our derivation of the energy-dependent real and imaginary potentials for spin-unsaturated, open j-shell even-even nuclei in the energy density model. In Sec. III, we discuss the role of spin density on our calculations of the optical potential, elastic scattering, and sub-barrier fusion. Finally, in Sec. IV, we present a summary of our conclusions.

II. DERIVATION OF ENERGY-DEPENDENT REAL AND IMAGINARY PARTS OF OPTICAL POTENTIAL FOR SPIN-UNSATURATED, OPEN j-SHELL NUCLEI

In the EDM, the energy-dependent real $V(D, E_{\text{c.m.}})$ and imaginary $W(D, E_{\text{c.m.}})$ parts of the optical potential of spin-unsaturated, open j-shell nuclei can be calculated as a function of their separation distance D and relative center-of-mass energy $E_{\text{c.m.}}$ as

$$V(D, E_{\text{c.m.}}) + iW(D, E_{\text{c.m.}}) = \int [H_c(\rho, \tau, J, E_{\text{c.m.}}) - H_1(\rho_1, \tau_1, J_1, E_{\text{c.m.}}) - H_2(\rho_2, \tau_2, J_2, E_{\text{c.m.}})] d^3R. \quad (1)$$

H_c, H_1, and H_2 are the energy-dependent complex Hamiltonian densities of the composite $(1+2)$ and individual systems of colliding nuclei (1) and (2). These can be obtained as a function of the matter density ρ, kinetic energy density τ, spin density $\vec{J}$, and center-of-mass energy $E_{\text{c.m.}}$ from a complex effective interaction v_c that should have a spin-orbit component.

In the present work, we have used the complex Skyrme effective interaction v_c for obtaining the complex Hamiltonian densities in Eq. (1):

$$v_c = (1 + i\gamma)v_{sky}, \quad (2)$$

where

$$v_{sky} = t_0(1 + x_0P_\sigma)\delta(\vec{r}) + \tfrac{1}{2}t_1[\delta(\vec{r})\vec{K}^2 + \vec{K'^2}\delta(\vec{r})] + t_2\vec{K'}.\delta(\vec{r})\vec{K} + \tfrac{1}{6}t_3(1 + P_\sigma)\rho\delta(\vec{r}) + iW_0(\vec{\sigma_1} + \vec{\sigma_2}) \cdot \vec{K'} \times \delta(\vec{r})\vec{K}. \quad (3)$$

t_0, t_1, t_2, t_3, x_0, and W_0 are the Skyrme interaction parameters [7]. $\vec{K} = (\vec{\nabla}_1 - \vec{\nabla}_2)/2i$ is the two-nucleon relative momentum acting on the wave function on the right and $\vec{K'}$ is adjoint of $\vec{K}$. $\vec{\sigma_1}$ and $\vec{\sigma_2}$ are the Pauli spin matrices and $P_\sigma = \frac{1}{2}(1 + \vec{\sigma_1} \cdot \vec{\sigma_2})$ is the spin exchange operator. The last term in Eq. (3) is the spin-orbit component of the Skyrme interaction.

The Fourier transform of the complex effective interaction v_c in Eq. (2) is given by the effective two-body matrix and the imaginary component γ of v_c is obtained in the forward scattering amplitude approximation [3] as

$$\gamma = -\hbar^2 k \langle\sigma\rangle / (2mJ). \quad (4)$$

In Eq. (4), m is the mass of the nucleon, and k, $\langle\sigma\rangle$, and J are the wave number of the incident nucleon, the average total nucleon-nucleon cross section inside the nucleus, and the volume integral of the two-body effective interaction v_{sky}, respectively. This is a valid approximation for the calculation of the imaginary potential W for a pair of heavy nuclei, where the large momentum transfers are cut down by the product of two nuclear form factors which are more forward peaked and the total energy of the projectile nucleon is scaled up due to its internal motion, which is now in an energy regime well above the Fermi energy, and the off-shell effect becomes less important [3].

In Eq. (1), the total energy

$$\int H_c d^3R = \sum_i \langle i|\frac{p^2}{2m}|i\rangle + \frac{1}{2}\sum_{i,j}[\langle ij|v_c|ij\rangle + \langle ij|v_c|ji\rangle] \quad (5)$$

of the colliding system can be expressed as the sum of the kinetic energy and potential energy. Here, i and j are the pairs of nucleons interacting through v_c. p is the momentum of the nucleon.

Assuming that the subspace of the occupied single-particle states is invariant under time reversal, and using the density matrix expansion (DME) of Negele and Vautherin [20], we obtain $H_c(\rho, \tau, J, E_{\text{c.m.}})$ in Eq. (1) as

$$\begin{aligned} H_c(\rho, \tau, J, E_{\text{c.m.}}) = {} & \frac{\hbar^2}{2m}\left[\frac{3}{5}K_F^2\rho + \frac{1}{36}\frac{(\nabla\rho)^2}{\rho} + \frac{1}{3}\nabla^2\rho\right] + (1 + i\gamma)\left\{\frac{3}{8}t_0\rho^2\left[1 - \frac{2}{3}\left(x_0 + \frac{1}{2}\right)\alpha^2\right] + \frac{1}{16}t_3\rho^3(1 - \alpha^2)\right. \\ & + \left\{\frac{1}{4}(t_1 + t_2)\rho + \frac{1}{32}(t_2 - t_1)\rho[(1 + \alpha)^{\frac{8}{3}} + (1 - \alpha)^{\frac{8}{3}}]\right\}\frac{3}{5}K_F^2\rho + \frac{\rho}{16}[3t_1 + 5t_2 + \alpha^2(t_2 - t_1)] \\ & \times \left[\frac{1}{36}\frac{(\nabla\rho)^2}{\rho} + \frac{1}{3}\nabla^2\rho\right] + \frac{1}{64}[5t_2 - 9t_1 + \alpha^2(3t_1 + t_2)] \times \rho\nabla^2\rho + \frac{1}{16}(t_1 - t_2)\left(\vec{J}_n^2 + \vec{J}_p^2\right) \\ & - \frac{1}{4}W_0\left[2\rho\vec{\nabla} \cdot \vec{J} + (1 + \alpha)\rho\vec{\nabla} \cdot \vec{J}_n + (1 - \alpha)\rho\vec{\nabla} \cdot \vec{J}_p\right] + \left[\left(\frac{2m}{\hbar^2}\right)^{1/2}\left(E_{c.m.1}^{1/2} + E_{c.m.2}^{1/2}\right)\right]^2 \\ & \left. \times \frac{1}{16}[3t_1 + 5t_2 + (t_2 - t_1)\alpha_1\alpha_2]\rho_1\rho_2\right\}, \end{aligned} \quad (6)$$

where α_1, α_2, and α are the neutron excess parameters of the individual nuclei (1) and (2) and the composite system (1 + 2), respectively. $E_{c.m.1}$ and $E_{c.m.2}$ are the translational energies of the target and projectile nucleons, respectively. The last term of Eq. (6) arises from the preservation of Galilean invariance of the interaction plus the linear dependence of τ on the relative center-of-mass energy $E_{\rm c.m.}$. The other consequence of the relative motion, i.e., the Pauli-blocking effect, is manifested through the Fermi momentum K_F obtained in the Fermi gas model [3]:

$$K_F^2 = (1.5\pi^2)^{\frac{2}{3}}\left[F\left(\rho_1^{\frac{5}{3}} + \rho_2^{\frac{5}{3}}\right) + (1-F)(\rho_1+\rho_2)^{\frac{5}{3}}\right]/\rho, \quad (7)$$

where F is the fractional volume of the Fermi sphere that does not overlap with the other fraction. The Hamiltonian densities H_1 and H_2 of nuclei (1) and (2) in Eq. (1) can be obtained from Eq. (6) by deleting the last term and by replacing ρ, τ, $\vec{J}$ by ρ_1, τ_1, $\vec{J}_1$ and ρ_2, τ_2, $\vec{J}_2$, respectively, and by substituting $F = 1$, $\rho_2 = 0$ and $F = 1$, $\rho_1 = 0$ in Eq. (7), respectively. Furthermore, in Eq. (6), the spin density $\vec{J} = \vec{J}_n + \vec{J}_p$, the nucleonic density $\rho = \rho_n + \rho_p$, and the kinetic energy density $\tau = \tau_n + \tau_p$. The subscripts n and p ($q = n, p$) refer to neutron and proton, respectively. The quantities ρ, τ, and $\vec{J}$, in turn, depend on the single-particle states ϕ_i:

$$\begin{aligned}
\rho_q(\vec{r}) &= \sum_{i,\sigma} |\phi_i(\vec{r},\sigma,q)|^2,\\
\tau_q(\vec{r}) &= \sum_{i,\sigma} |\nabla\phi_i(\vec{r},\sigma,q)|^2, \quad (8)\\
\vec{J_q}(r) &= (-i)\sum_{i,\sigma,\sigma'} \phi_i^*(\vec{r},\sigma,q)[\vec{\nabla}\phi_i(\vec{r},\sigma',q)\times\langle\sigma|\vec{\sigma}|\sigma'\rangle].
\end{aligned}$$

Here, $\vec{r}$, σ, and q are the space, spin, and isospin coordinates of the nucleon. The sums in Eq. (8) are taken over all the occupied single-particle states:

$$\phi_i(r,\sigma,q) = \frac{R_\alpha(r)}{r} Y_{ljm}(\vec{r},\sigma)\chi_q(t), \quad (9)$$

where

$$Y_{ljm}(\vec{r},\sigma) = \sum_{m_l m_s} \left\langle l\tfrac{1}{2} m_l m_s \middle| jm\right\rangle Y_{lm_l}(\vec{r})\chi_{m_s}(\sigma). \quad (10)$$

l, s, j, and m refer to orbital angular momentum, spin, total angular momentum, and magnetic quantum number. $\chi_q(t)$ and $\chi_{m_s}(\sigma)$ are the isospin and spin parts of the wave function. The notation $\alpha \equiv q, n, l$ specifies the radial part of the wave function $R_\alpha(r)$ with n as the principal quantum number.

The contribution of ϕ_i toward the spin density $\vec{J}_q(\vec{r})$ in Eq. (8) for the open j-shell nucleus is divided into two parts, one due to the core consisting of closed l or j shell and other due to the valence N nucleons in the last occupied j shell:

$$\vec{J}_q(\vec{r}) = \vec{J}_c(\vec{r}) + \vec{J}_N(\vec{r}), \quad (11)$$

where

$$\begin{aligned}
\vec{J}_C(\vec{r}) = \frac{\vec{r}}{4\pi r^4}\sum_\alpha (2j_\alpha+1)\\
\times\left[j_\alpha(j_\alpha+1) - l_\alpha(l_\alpha+1) - \frac{3}{4}\right]R_\alpha^2(r) \quad (12)
\end{aligned}$$

and

$$\vec{J}_N(\vec{r}) = \frac{N\vec{r}}{4\pi r^4}\left[j(j+1) - l(l+1) - \frac{3}{4}\right]R_\alpha^2(r). \quad (13)$$

In Eqs. (12) and (13), j, l, and α correspond to the last occupied but partially filled j shell only. For a completely filled l-shell nucleus (such as ^{16}O), $\vec{J}_c = 0$, and for a completely filled (closed) j-shell [$N = (2j+1)$] nucleus (such as ^{12}C), $\vec{J}_N = \vec{J}_c$. Similar expressions for ρ and τ can also be obtained [9,20] for the open j-shell nucleus. Instead, we have used the approximation made by Stancu and Brink [8] for τ in Eq. (6):

$$\tau = \frac{3}{5}K_f^2\rho + \frac{1}{36}\frac{(\nabla\rho)^2}{\rho} + \frac{1}{3}\nabla^2\rho. \quad (14)$$

Consequently, H_c in Eq. (6) is expressed in terms of ρ and $\vec{J}$.

The nucleonic densities ρ of all the spin-unsaturated and spin-saturated nuclei considered here are taken from the experimental works [16,17,21], which are supposed to contain the contributions from space, spin, and isospin parts of the wave function in Eq. (8). Any self-consistent calculation with a suitable effective interaction guarantees the reproduction of the experimental nucleonic density distribution. Furthermore, it has been shown that, in the surface region, the experimental nucleonic density gives heavy-ion potentials identical to the one obtained from the shell-model wave functions [12–15]. We have, therefore, used the normalized (shell-model) radial wave functions $\phi_{nl} = \frac{R_\alpha}{r}$ based on the harmonic oscillator potential [22], with shell-model configurations of neutrons and protons presented in Table I to obtain the spin density $\vec{J}_q(\vec{J}_n, \vec{J}_p)$ in Eq. (8) for the spin-unsaturated closed j-shell [Eq. (12)] and open j-shell [Eq. (13)] nuclei studied here as

$$\begin{aligned}
\vec{J}_n &= \hat{u}\frac{8}{3\pi^{\frac{3}{2}}}\frac{r}{b^5}\exp(-r^2/b^2) \quad (^{12}\mathrm{C})\\
&= \hat{u}\frac{16}{15\pi^{\frac{3}{2}}}\frac{r^3}{b^7}\exp(-r^2/b^2) \quad (^{18}\mathrm{O},^{20}\mathrm{Ne})\\
&= \hat{u}\frac{32}{15\pi^{\frac{3}{2}}}\frac{r^3}{b^7}\exp(-r^2/b^2) \quad (^{24}\mathrm{Mg})\\
&= \hat{u}\frac{16}{5\pi^{\frac{3}{2}}}\frac{r^3}{b^7}\exp(-r^2/b^2) \quad (^{32}\mathrm{S})\\
&= \hat{u}\frac{8}{5\pi^{\frac{3}{2}}}\frac{r^3}{b^7}\exp(-r^2/b^2) \quad (^{34}S)\\
&= \hat{u}\frac{16}{35\pi^{\frac{3}{2}}}\frac{r^5}{b^9}\exp(-r^2/b^2) \quad (^{42}\mathrm{Ca})\\
&= \hat{u}\frac{32}{35\pi^{\frac{3}{2}}}\frac{r^5}{b^9}\exp(-r^2/b^2) \quad (^{44}\mathrm{Ca})\\
&= \hat{u}\frac{64}{35\pi^{\frac{3}{2}}}\frac{r^5}{b^9}\exp(-r^2/b^2) \quad (^{52}\mathrm{Cr},^{54}\mathrm{Fe})\\
&= \hat{u}\left[\frac{64}{35\pi^{\frac{3}{2}}}\frac{r^5}{b^9} + \frac{10}{3\pi^{\frac{3}{2}}}\frac{r}{b^5}\left(1-\frac{2}{5}\frac{r^2}{b^2}\right)^2\right]\\
&\quad\times\exp(-r^2/b^2) \quad (^{58}\mathrm{Ni})
\end{aligned}$$

TABLE I. Shell-model configurations of protons (p) and neutrons (n) in the last $j_{p,n} = l_{p,n} \pm \frac{1}{2}$ shells of colliding nuclei considered in the present work.

Nucleus	Proton state	l_p	$j_p = l_p + \frac{1}{2}$	$j_p = l_p - \frac{1}{2}$	Neutron state	l_n	$j_n = l_n + \frac{1}{2}$	$j_n = l_n - \frac{1}{2}$
^{12}C	$(1p_{3/2})^4$	open	closed	–	$(1p_{3/2})^4$	open	closed	–
^{16}O	$(1p_{1/2})^2$	closed	closed	closed	$(1p_{1/2})^2$	closed	closed	closed
^{18}O	$(1p_{1/2})^2$	closed	closed	closed	$(1d_{5/2})^2$	open	open	–
^{20}Ne	$(1d_{5/2})^2$	open	open	–	$(1d_{5/2})^2$	open	open	–
^{24}Mg	$(1d_{5/2})^4$	open	open	–	$(1d_{5/2})^4$	open	open	–
^{32}S	$(2s_{1/2})^2$	open	closed	–	$(2s_{1/2})^2$	open	closed	–
^{34}S	$(2s_{1/2})^2$	open	closed	–	$(1d_{3/2})^2$	open	closed	open
^{36}S	$(2s_{1/2})^2$	open	closed	–	$(1d_{3/2})^4$	closed	closed	closed
^{42}Ca	$(1d_{3/2})^4$	closed	closed	closed	$(1f_{7/2})^2$	open	open	–
^{44}Ca	$(1d_{3/2})^4$	closed	closed	closed	$(1f_{7/2})^4$	open	open	–
^{52}Cr	$(1f_{7/2})^4$	open	open	–	$(1f_{7/2})^8$	open	closed	–
^{54}Fe	$(1f_{7/2})^6$	open	open	–	$(1f_{7/2})^8$	open	closed	–
^{58}Ni	$(1f_{7/2})^8$	open	closed	–	$(2p_{3/2})^2$	open	open	–
^{60}Ni	$(1f_{7/2})^8$	open	closed	–	$(2p_{3/2})^4$	open	closed	–
^{62}Ni	$(1f_{7/2})^8$	open	closed	–	$(1f_{5/2})^2$	open	closed	open
^{64}Ni	$(1f_{7/2})^8$	open	closed	–	$(1f_{5/2})^4$	open	closed	open
^{74}Ge	$(2p_{3/2})^4$	open	closed	–	$(1g_{9/2})^2$	open	open	–
^{76}Ge	$(2p_{3/2})^4$	open	closed	–	$(1g_{9/2})^4$	open	open	–
^{92}Zr	$(2p_{1/2})^2$	closed	closed	closed	$(1g_{7/2})^2$	open	closed	open

$$
\begin{aligned}
&= \hat{u}\left[\frac{64}{35\pi^{\frac{3}{2}}}\frac{r^5}{b^9} + \frac{20}{3\pi^{\frac{3}{2}}}\frac{r}{b^5}\left(1-\frac{2}{5}\frac{r^2}{b^2}\right)^2\right] \\
&\quad \times \exp(-r^2/b^2) \quad (^{60}\mathrm{Ni}) \\
&= \hat{u}\left[\frac{128}{105\pi^{\frac{3}{2}}}\frac{r^5}{b^9} + \frac{20}{3\pi^{\frac{3}{2}}}\frac{r}{b^5}\left(1-\frac{2}{5}\frac{r^2}{b^2}\right)^2\right] \\
&\quad \times \exp(-r^2/b^2) \quad (^{62}\mathrm{Ni}) \\
&= \hat{u}\left[\frac{64}{105\pi^{\frac{3}{2}}}\frac{r^5}{b^9} + \frac{20}{3\pi^{\frac{3}{2}}}\frac{r}{b^5}\left(1-\frac{2}{5}\frac{r^2}{b^2}\right)^2\right] \\
&\quad \times \exp(-r^2/b^2) \quad (^{64}\mathrm{Ni}) \\
&= \hat{u}\frac{128}{945\pi^{\frac{3}{2}}}\frac{r^7}{b^{11}}\exp(-r^2/b^2) \quad (^{74}\mathrm{Ge}) \\
&= \hat{u}\frac{256}{945\pi^{\frac{3}{2}}}\frac{r^7}{b^{11}}\exp(-r^2/b^2) \quad (^{76}\mathrm{Ge}) \\
&= \hat{u}\left[\frac{128}{189\pi^{\frac{3}{2}}}\frac{r^7}{b^{11}} + \frac{56}{15\pi^{\frac{3}{2}}}\frac{r^3}{b^7}\left(1-\frac{2}{7}\frac{r^2}{b^2}\right)^2\right] \\
&\quad \times \exp(-r^2/b^2) \ (^{92}\mathrm{Zr}), \qquad (15)
\end{aligned}
$$

where $\hat{u}$ is the unit vector in the radial direction and b is the oscillator length.

From the shell-model configuration of protons inside a nucleus, presented in Table I, one can ascertain that the expression for $\vec{J}_p$ of all the colliding nuclei can be obtained from $\vec{J}_n$ in Eq. (15). In Eq. (1), the spin densities $\vec{J}_1$ and $\vec{J}_2$ for nuclei (1) and (2) are thus obtained from Eq. (15) as $\vec{J}_1 = \vec{J}_{n1} + \vec{J}_{p1}$ and $\vec{J}_2 = \vec{J}_{n2} + \vec{J}_{p2}$, and the spin density $\vec{J}$ of the composite system (1 + 2) is obtained in the sudden approximation, i.e., $\vec{J} = \vec{J}_1 + \vec{J}_2$.

In order to study the role of both the spin-density terms,

$$
\begin{aligned}
&\tfrac{1}{16}(t_1 - t_2)\left(\vec{J}_n^2 + \vec{J}_p^2\right) - \tfrac{1}{4}W_0[2\rho\vec{\nabla}\cdot\vec{J} \\
&\quad + (1+\alpha)\rho\vec{\nabla}\cdot\vec{J}_n + (1-\alpha)\rho\vec{\nabla}\cdot\vec{J}_p], \qquad (16)
\end{aligned}
$$

of the Skyrme energy density H_c in Eq. (6) on the estimation of the potentials V_E and W_E, we have excluded these terms from H_c and computed the potentials, denoted as V_N and W_N. Then, the spin-density contributions are $V_J = V_E - V_N$ and $W_J = W_E - W_N$, respectively, toward the real V_E and imaginary W_E potentials. Note that the term $\frac{1}{16}(t_2 - t_1)(\vec{J}_n^2 + \vec{J}_p^2)$ is the contribution of the central (Wigner) component of the Skyrme interaction whereas the term $\frac{1}{4}W_0[2\rho\vec{\nabla}\cdot\vec{J} + (1+\alpha)\rho\vec{\nabla}\cdot\vec{J}_n + (1-\alpha)\rho\vec{\nabla}\cdot\vec{J}_p]$ is the contribution of the spin-orbit component of the Skyrme interaction. Both terms vanish for a spin-saturated or completely filled l-shell nucleus, i.e., when $\vec{J}_n = \vec{J}_p = 0$. These terms will contribute toward the potentials V and W in Eq. (1) only when one of the j shells of the last l shell of either one or both of the colliding nuclei are completely filled up, i.e., $\vec{J}_c \neq 0$, or partially filled up, i.e., $\vec{J}_N \neq 0$.

It may be mentioned that the DME of Negele and Vautherin is exact when one uses a short-range effective interaction [4]. Thus, it enables one to obtain the Skyrme-Hartree-Fock energy density in Eq. (6) exactly [9].

III. CALCULATIONS AND RESULTS

A. Optical potential of open j-shell nuclei

We have considered from Table I reactions of some twenty pairs of nuclei, with at least one of the interacting nuclei having an open j shell.

TABLE II. Numerical values of the inter-ion separation distance D_t, D_{ma}, D_s, D_i, and D_w, as defined in the text, and the percentage contributions $\Delta V_J(D_{ma})$, $\Delta V_J(D_s)$, $\Delta W_J(D_i)$, and $\Delta W_J(D_w)$ of the spin-density terms toward the potentials V_E and W_E at these distances.

System	$E_{\text{c.m.}}$ (MeV)	D_t (fm)	D_{ma} (fm)	$\Delta V_J(D_{ma})$	D_s (fm)	$\Delta V_J(D_s)$	D_i (fm)	$\Delta W_J(D_i)$	D_w (fm)	$\Delta W_J(D_w)$
$^{16}O + ^{20}Ne$	30.88	3.9	4.4	2.52	4.4	1.86	5.7	2.56	5.7	2.56
$^{16}O + ^{42}Ca$	43.45	4.5	5.5	0.86	5.7	0.83	6.2	1.45	6.7	1.03
$^{16}O + ^{44}Ca$	44	4.5	5.5	1.67	5.7	1.62	6.2	3.01	6.7	2.02
$^{16}O + ^{52}Cr$	45.88	4.1	5.3	8.19	5.8	6.44	6.7	5.83	7.0	4.71
$^{16}O + ^{54}Fe$	46.29	4.1	5.3	9.78	5.8	9.40	6.7	6.69	7.0	5.45
$^{16}O + ^{58}Ni$	47.03	4.2	5.3	9.67	5.8	7.92	6.9	8.28	7.2	5.10
$^{16}O + ^{62}Ni$	47.69	4.0	5.2	11.96	6.0	6.43	6.9	5.41	7.2	4.33
$^{16}O + ^{64}Ni$	48	4.0	5.2	9.76	6.0	5.15	6.9	4.35	7.2	3.36
$^{16}O + ^{74}Ge$	46.04	4.1	5.3	10.83	6.3	4.04	7.1	3.62	7.5	2.53
$^{16}O + ^{76}Ge$	46.26	4.2	5.4	8.82	6.2	5.17	7.2	4.20	7.5	3.31
$^{16}O + ^{92}Zr$	47.70	4.4	5.6	9.52	6.6	3.77	7.5	3.02	7.9	2.17
$^{18}O + ^{60}Ni$	48.46	4.3	5.5	10.15	5.9	9.02	6.8	11.24	7.3	8.93
$^{18}O + ^{62}Ni$	48.82	4.2	5.5	11.29	6.1	8.14	6.9	9.23	7.3	8.060
$^{18}O + ^{64}Ni$	49.17	4.3	5.5	8.40	6.1	8.30	6.8	9.06	7.3	5.58
$^{18}O + ^{76}Ge$	45.28	4.5	5.8	7.56	6.3	6.23	7.1	8.90	7.6	5.58
$^{24}Mg + ^{32}S$	68.57	4.1	5.2	10.54	5.3	10.45	6.1	17.98	6.7	11.31
$^{32}S + ^{34}S$	49.97	4.3	5.5	11.74	5.7	11.32	6.6	14.39	7.1	9.70
$^{24}Mg + ^{36}S$	72	4.3	5.2	6.5	5.5	6.09	6.2	12.42	6.8	7.77
$^{12}C + ^{62}Ni$	40.22	4.2	5.4	18.06	5.9	13.45	6.5	19.32	6.9	13.10
$^{58}Ni + ^{64}Ni$	114.9	5.1	6.6	16.89	7.3	12.33	8.4	12.04	8.8	8.86

(i) In ten cases, the projectile is a spin-saturated, doubly l-closed shell nucleus ^{16}O, with the targets (a) having proton and neutron orbitals as l-closed, j-open ^{42}Ca, ^{44}Ca, and ^{92}Zr; (b) l-open (j-closed), j-open ^{58}Ni, ^{62}Ni, ^{64}Ni, ^{74}Ge, and ^{76}Ge; (c) j-open, l-open (j-closed) ^{52}Cr and ^{54}Fe; and (d) j-open, j-open ^{20}Ne.

(ii) In the second type, the projectile ^{18}O has proton and neutron orbitals as l-closed, j-open and the targets are (a) l-open, l-open ^{60}Ni and (b) l-open, j-open shell ^{62}Ni, ^{64}Ni, ^{74}Ge, and ^{76}Ge nuclei.

(iii) In the third type, the projectile is ^{58}Ni and the target ^{64}Ni is an l-open, j-open shell nucleus.

(iv) In the fourth type, the projectiles ^{12}C and ^{32}S are doubly l-open shell nuclei and the targets ^{62}Ni and ^{34}S are l-open, j-open shell nuclei.

(v) Finally, the projectile ^{24}Mg has both neutron and proton orbitals as j-open and the targets are (a) l-open, l-closed ^{36}S and (b) l-open, l-open shell ^{32}S nuclei.

Such a wide range of combinations of interacting nuclei, with respect to their neutron and proton spin densities $\vec{J}_n$ and $\vec{J}_p$ [Eq. (15)] arising from n, l, and $j = l \pm \frac{1}{2}$ values, presented in Table I, will enable us to study systematically the role of spin-density terms of the Skyrme III energy density in their determination of the elastic scattering optical potential of open j-shell nuclei.

We have computed the energy-dependent real $V_E(D, E_{\text{c.m.}})$, $V_N(D, E_{\text{c.m.}})$, and $V_J(D, E_{\text{c.m.}})$ and imaginary $W_E(D, E_{\text{c.m.}})$, $W_N(D, E_{\text{c.m.}})$, and $W_J(D, E_{\text{c.m.}})$ parts of the elastic scattering optical potential derived in the previous section for all twenty pairs of open j-shell nuclei studied here, using the Set III parameters of the Skyrme interaction [7], the experimental nucleonic densities ρ_1 and ρ_2 from [16,17,21] for the nuclei (1) and (2), and $\rho = \rho_1 + \rho_2$ for the composite system (1 + 2).

Table II shows the results of our calculation for all twenty pairs of open j-shell nuclei studied here, and Figs. 1–6 show the same for six pairs of nuclei, i.e., $^{12}C + ^{62}Ni$ ($E_{\text{c.m.}} = 40.22$ MeV), $^{16}O + ^{54}Fe$ ($E_{\text{c.m.}} = 46.29$ MeV), $^{18}O + ^{60}Ni$ ($E_{\text{c.m.}} = 48.46$ MeV), $^{24}Mg + ^{32}S$ ($E_{\text{c.m.}} = 68.57$ MeV), $^{32}S + ^{34}S$ ($E_{\text{c.m.}} = 49.97$ MeV), and $^{58}Ni + ^{64}Ni$ ($E_{\text{c.m.}} = 114.99$ MeV). We notice in Figs. 1 and 2

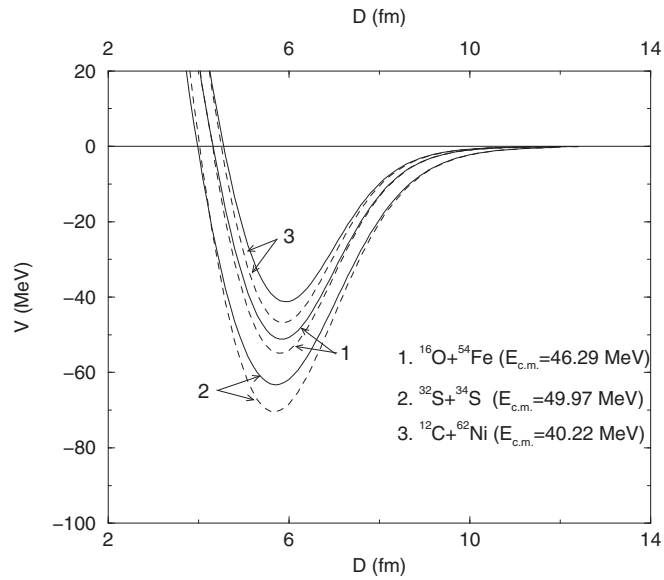

FIG. 1. Effect of spin density terms on the real part of the energy-dependent optical potential of the colliding nuclei: V_E (solid line); V_N (dashed line).

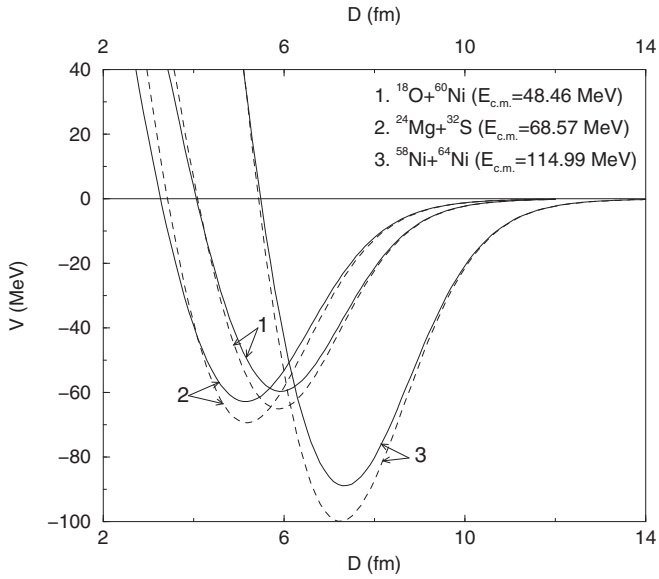

FIG. 2. Effect of spin density terms on the real part of the energy-dependent optical potential of the colliding nuclei: V_E (solid line); V_N (dashed line).

that, at the smaller separation distance D, the potential V_E is more attractive than the potential V_N, but, as D increases, the potential V_N is found to be more attractive than the potential V_E. This transition from attractive to repulsive behavior, due to the spin-density potential V_J, occurs at a separation distance $D = D_t$, given in Table II. Beyond D_t, the potential V_J increases and reaches a maximum at D_{ma} and thereafter it decreases gradually to zero, as shown explicitly in Fig. 3. The maxima occurs inside the minima D_s of the potential V_E.

The percentage contribution $\Delta V_J = 100 V_J / V_E$ at the maximum D_{ma} of the spin-density potential V_J is always larger than at the minimum D_s of the potential V_E (presented in Table II). At the repulsive maximum D_{ma}, the contribution of the spin-density terms is found to be very large and reduces

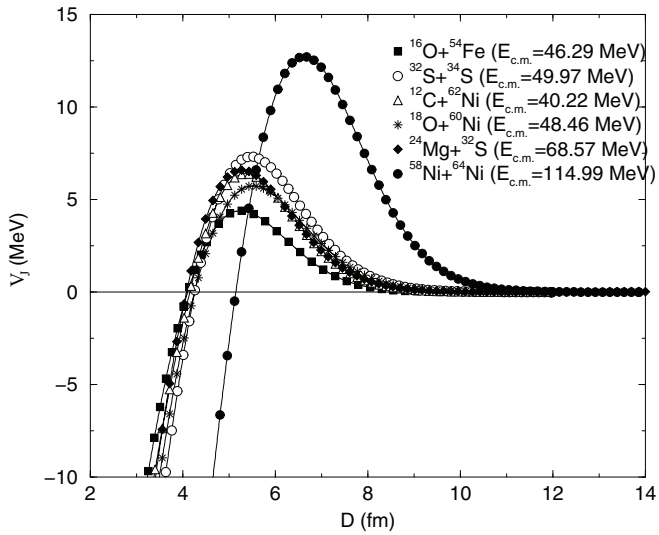

FIG. 3. Contribution of the spin density terms toward the real part of the energy-dependent optical potential of the colliding nuclei.

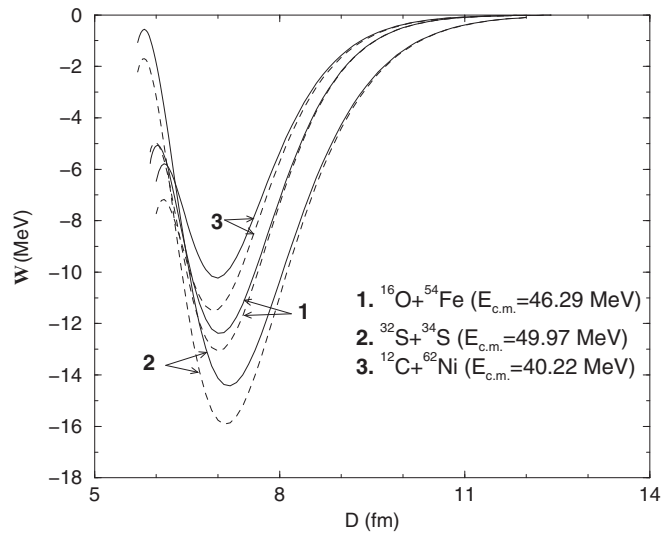

FIG. 4. Effect of spin density terms on the imaginary part of the energy-dependent optical potential of the colliding nuclei: W_E (solid line); W_N (dashed line).

the potential V_E by up to 18% in case of ^{12}C + ^{62}Ni and by about 17% in case of ^{58}Ni + ^{64}Ni.

The values of D_t, D_{ma}, D_s, $V_J(D_t)$, $V_E(D_{ma})$, and $V_E(D_s)$ play a very important role in determining the characteristics of transfer reactions of spin-unsaturated nuclei [13–15]. Figures 4 and 5 show that the imaginary potential W_E is absorptive for all values of D. On the other hand, Fig. 6 shows that the spin-density imaginary potential W_J is emissive at a short distance D, followed by a well and a maximum at D_i, before approaching zero at a large D. In a few cases, such as ^{16}O + ^{54}Fe, ^{18}O + ^{60}Ni, and ^{58}Ni + ^{64}Ni, the pocket of W_J drops below the zero axis and becomes strongly absorptive. The maxima of W_J at D_i, in all cases, occurs inside the minimum of the potential W_E at D_w. Table II shows that the

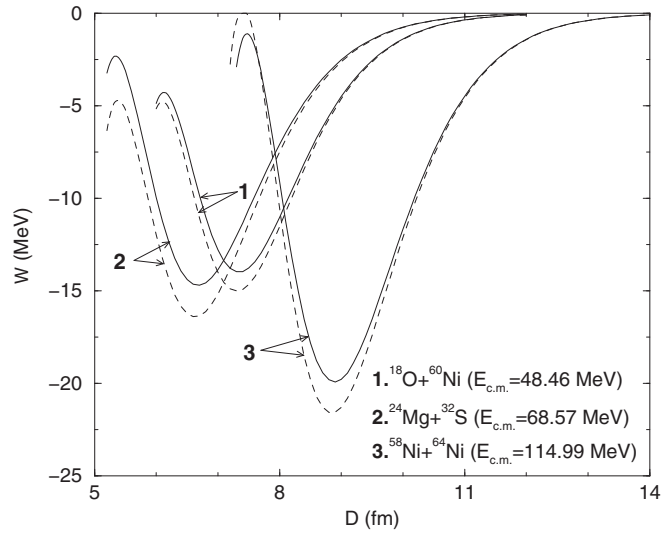

FIG. 5. Effect of spin density terms on the imaginary part of the energy-dependent optical potential of the colliding nuclei: W_E (solid line); W_N (dashed line).

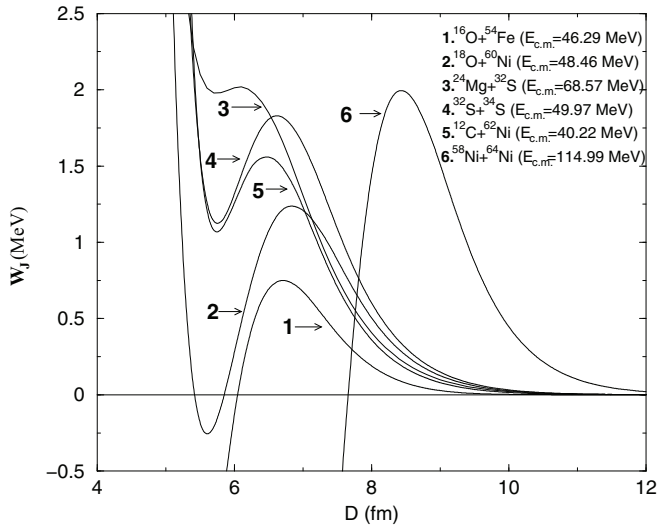

FIG. 6. Contribution of spin density terms toward the imaginary part of the energy-dependent optical potential of the colliding nuclei.

percentage contribution $\Delta W_J = 100 W_J / W_E$ of the potential W_J toward the potential W_E at D_i is larger than at D_w. At the emissive maximum D_i, the contribution of the spin-density terms is found to be very large and reduces the potential W_E by up to about 19% in case of $^{12}\mathrm{C} + {}^{62}\mathrm{Ni}$. However, the values of D_t, D_{ma}, and D_s are smaller than the sum of the half-density radii R_{12} of the colliding nuclei (1) and (2).

It may be noted that the potentials V_E, W_E and V_N, W_N and V_J, W_J, calculated in sudden approximation ($\rho = \rho_1 + \rho_2$, $\vec{J} = \vec{J}_1 + \vec{J}_2$), are not reliable quantitatively at the above-noted distances since, in the interior region of $D < R_{12}$, there will be a strong overlap of the projectile and target densities. Under the sudden approximation, the overlap density $\rho = \rho_1 + \rho_2$ in this region exceeds the normal nuclear matter density $\rho_{nm} = 0.17\ \mathrm{fm}^{-3}$, for which the Skyrme effective interaction used here is not determined. Thus, the exit channel events occurring due to the potentials in the strong overlap region ($D < R_{12}$) may not be explained properly by the potentials calculated under such an approximation. Therefore, in the following, we have studied the role of spin-density terms of the Skyrme energy density [Eq. (16)] in the calculation of the potentials V_E and W_E in the region of weak overlap ($D \geqslant R_{12}$) where the density ρ does not exceed the normal nuclear matter density ρ_{nm}.

The percentage contributions of the spin-density terms ΔV_J and ΔW_J toward the potentials V_E and W_E at $D \geqslant R_{12}$ are presented in Table III. A cursory inspection of the results reveals the following: (i) For a fixed l, ΔV_J and ΔW_J increase when the number of valence nucleons occupying the same (fixed) orbital $j = l + \frac{1}{2}$ increases. (ii) For a fixed l, ΔV_J and ΔW_J decrease when the number of valence nucleons occupying the same (fixed) orbitals $j = l - \frac{1}{2}$ is more. The number of holes in the last $j = l - \frac{1}{2}$ shell decreases, and the nucleus tends toward the closure of the l shell. (iii) ΔV_J and ΔW_J increase when the valence nucleons are at the higher n or l orbitals. (iv) ΔV_J and ΔW_J increase when more neutron and proton orbitals of the projectile and the target nuclei remain unsaturated. (v) For each colliding system, ΔW_J is larger than ΔV_J at $D \geqslant R_{12}$. In this region, ΔV_J and ΔW_J are repulsive and have maximum values at $D = R_{12}$, and they decrease gradually to zero as D increases. Among the twenty pairs of nuclei considered in this work, the pairs of doubly spin-unsaturated shell nuclei ($^{12}\mathrm{C} + {}^{62}\mathrm{Ni}$, $^{24}\mathrm{Mg} + {}^{32}\mathrm{S}$, $^{32}\mathrm{S} + {}^{34}\mathrm{S}$, and $^{58}\mathrm{Ni} + {}^{64}\mathrm{Ni}$) make larger spin-density contributions ΔV_J and ΔW_J toward their interaction potential in the region of $D > R_{12}$, the maximum contributions being $\Delta V_J = 9.6\%$ and $\Delta W_J = 17.4\%$ in the case of $^{12}\mathrm{C} + {}^{62}\mathrm{Ni}$ at $D = R_{12}$. As the heavy-ion interaction potential at $D \geqslant R_{12}$ causes elastic scattering and fusion of colliding nuclei in the exit channel, we investigate the effect of the spin-density potentials V_J and W_J of the aforementioned twenty pairs of open j-shell nuclei on these quantities in the following.

B. Elastic scattering

The ratios σ_{el}/σ_R of the elastic scattering cross section σ_{el} to Rutherford cross section σ_R of all the pairs of open j-shell nuclei are computed from the calculated optical potentials $V_E + iW_E$ and $V_N + iW_N$, respectively, with and without spin-density terms. It is found that the calculated potentials $V_E + iW_E$ reproduce nicely the experimental data on scattering cross sections [23–33] for all the pairs of nuclei studied, without any renormalization. Some of these results are shown in Figs. 7 and 8. The shape of σ_{el}/σ_R deviates from a straight line at the center-of-mass angle $\theta = \theta_i$ and shows a number of oscillations about the Rutherford value, with increasing amplitude, up to a maxima at the angle $\theta = \theta_m$, followed by a sharp fall in the forward angle regime. The potential $V_N + iW_N$, without spin-density terms, also gives an identical shape of σ_{el}/σ_R, fitting the data equally nicely. In the angular region $\theta_i \leqslant \theta \leqslant \theta_m$, both sets of potentials $V_E + iW_E$ and $V_N + iW_N$ predict almost identical variations of σ_{el}/σ_R, including the position of the maxima at θ_m and the height of the maxima. There are small differences, of up to about 1%, between their values of σ_{el}/σ_R at $\theta > \theta_m$. As the oscillating structure of the elastic scattering cross sections σ_{el}/σ_R is reminiscent of a Fresnel diffractive pattern in the forward angle regime, the dominating feature of such a collision is the strong absorption from the elastic channel within a well-defined geometrical region.

The ratio σ_{el}/σ_R defines strong absorption with different proportions and determines the radial distance D of this region of the optical potential, sensitive to elastic scattering,

$$D = \eta \frac{\lambda}{2\pi} \left(1 + \mathrm{cosec}\frac{1}{2}\theta\right), \tag{17}$$

where η and λ are the Coulomb parameter and the de Broglie wavelength of the reacting partners. At the angle $\theta = \theta_i$, the nuclear potential starts manifesting and the elastic scattering cross section σ_{el} deviates from its Rutherford values σ_R and achieves its maximum value at the angle $\theta = \theta_m$. It reduces to $1/2$, $1/4$, and $1/100$ of the Rutherford cross section at $\theta = \theta_{1/2}$, $\theta_{1/4}$, and $\theta_{1/100}$. The absorption of incident flux is 50%, 75%, and 99%, respectively, in the reaction channel at these angles. Practically, there is no scattering beyond $\theta = \theta_{1/100}$. These

TABLE III. Percentage contributions ΔV_J and ΔW_J of the spin-density terms toward the real V_E and imaginary W_E parts of the optical potential of the interacting systems at different values of the separation distance $D \geqslant R_{12}$.

System	$E_{\text{c.m.}}$ (MeV)	R_{12} (fm)	Potential	$D = R_{12}$	7 fm	8 fm	9 fm	10 fm	11 fm	12 fm
$^{16}O + ^{20}Ne$	30.88	5.46	ΔV_J	2.692	1.91	1.16	0.54	0.20	0.06	0.02
			ΔW_J	2.708	1.95	1.36	0.91	0.58	0.33	0.14
$^{16}O + ^{42}Ca$	43.45	6.46	ΔV_J	0.909	0.91	0.87	0.67	0.36	0.12	0.03
			ΔW_J	1.154	0.93	0.87	0.86	0.81	0.69	0.54
$^{16}O + ^{44}Ca$	44	6.52	ΔV_J	1.743	1.74	1.65	1.30	0.70	0.24	0.05
			ΔW_J	2.233	1.82	1.72	1.63	1.54	1.33	0.96
$^{16}O + ^{52}Cr$	45.88	6.64	ΔV_J	4.075	3.30	1.77	0.87	0.38	0.14	0.04
			ΔW_J	6.046	4.71	2.10	1.07	0.59	0.35	0.24
$^{16}O + ^{54}Fe$	46.28	6.73	ΔV_J	4.483	3.87	2.14	0.99	0.33	0.06	0.003
			ΔW_J	6.558	5.45	2.64	1.27	0.55	0.22	0.06
$^{16}O + ^{58}Ni$	47.03	6.93	ΔV_J	4.227	4.05	2.09	1.01	0.45	0.17	0.06
			ΔW_J	6.169	5.90	2.56	1.21	0.61	0.33	0.21
$^{16}O + ^{62}Ni$	47.69	6.92	ΔV_J	3.558	3.38	1.74	0.77	0.25	0.05	0.00
			ΔW_J	5.342	5.04	2.27	0.99	0.39	0.14	0.07
$^{16}O + ^{64}Ni$	48	6.87	ΔV_J	2.746	2.49	1.17	0.52	0.22	0.08	0.02
			ΔW_J	4.442	4.02	1.52	0.64	0.30	0.15	0.09
$^{16}O + ^{74}Ge$	46.04	7.10	ΔV_J	2.122	–	1.03	0.46	0.19	0.08	0.02
			ΔW_J	3.624	–	1.50	0.60	0.27	0.13	0.06
$^{16}O + ^{76}Ge$	46.26	7.28	ΔV_J	2.434	–	1.43	0.67	0.30	0.12	0.04
			ΔW_J	3.969	–	2.04	0.85	0.40	0.20	0.10
$^{16}O + ^{92}Zr$	47.70	7.54	ΔV_J	1.861	–	1.31	0.56	0.19	0.05	0.00
			ΔW_J	2.927	–	1.97	0.77	0.27	0.07	0.00
$^{18}O + ^{60}Ni$	48.46	7.01	ΔV_J	5.849	–	3.85	2.50	1.56	0.88	0.44
			ΔW_J	9.365	–	4.56	2.78	1.93	1.43	1.09
$^{18}O + ^{62}Ni$	48.83	6.95	ΔV_J	5.453	5.33	3.50	2.30	1.40	0.75	0.34
			ΔW_J	8.817	8.44	4.08	2.58	1.83	1.34	0.98
$^{18}O + ^{64}Ni$	49.17	6.90	ΔV_J	4.929	4.24	2.83	1.92	1.25	0.75	0.40
			ΔW_J	8.093	7.31	3.38	2.14	1.56	1.20	0.95
$^{18}O + ^{76}Ge$	45.28	7.31	ΔV_J	4.156	–	3.18	2.20	1.47	0.90	0.49
			ΔW_J	7.168	–	4.15	2.46	1.74	1.32	1.02
$^{24}Mg + ^{32}S$	68.57	6.24	ΔV_J	9.40	7.55	5.24	3.41	2.06	1.12	0.55
			ΔW_J	15.673	9.43	5.75	3.93	2.83	2.09	1.57
$^{32}S + ^{34}S$	49.97	6.63	ΔV_J	8.545	7.42	4.87	3.09	1.89	1.08	0.55
			ΔW_J	16.625	11.61	5.80	3.48	2.31	1.64	1.24
$^{24}Mg + ^{36}S$	72	6.44	ΔV_J	6.109	5.37	3.94	2.67	1.67	0.94	0.47
			ΔW_J	9.880	6.93	4.28	2.98	2.18	1.63	1.22
$^{12}C + ^{62}Ni$	40.22	6.60	ΔV_J	9.645	8.19	5.73	3.94	2.40	1.25	0.56
			ΔW_J	17.418	11.99	6.72	5.05	4.14	3.41	2.87
$^{58}Ni + ^{64}Ni$	114.99	8.49	ΔV_J	8.958	–	–	5.37	3.24	1.98	1.20
			ΔV_J	14.224	–	–	7.61	3.81	2.26	1.47

angles are used in Eq. (17) to obtain the corresponding radial distances D_i, D_m, $D_{1/2}$, $D_{1/4}$, and $D_{1/100}$. Our results show that $D_i > D_m > D_{1/2} > D_{1/4} > D_{1/100} > R_{12}$. As the colliding nuclei approach each other, there is more absorption from the incident channel and their elastic scattering cross section σ_{el} decreases. The scattering disappears just after $D_{1/100}$ before the colliding nuclei touch each other at R_{12}. The geometrical region $D_i > D > D_{1/100}$ of the optical potential, sensitive to elastic scattering, is found to be about 6 fm wide whereas the strong absorption from the elastic channel corresponds to a radial region $D_m > D > D_{1/100}$ of about 4 fm.

We have also calculated the contributions of ΔV_J and ΔW_J of the spin-density terms in the well-defined geometrical region $D_i > D > D_{1/100}$. Our results, presented in Table IV, reveal that the contributions in this geometrical region are appreciable for several pairs of open j-shell nuclei. In case of $^{12}C + ^{62}Ni$, ΔV_J and ΔW_J at $D_{1/100}$ are found to be 6% and 7%, respectively, but the contribution varies with the distance D. When the scattering is dominant at θ_m, these contributions are small at the corresponding distance $D = D_m$. The contribution increases slowly in the region $D < D_m$ with rapid depletion of the scattering cross section. It achieves maximum value at $D = D_{1/100}$ where there is almost complete 99% absorption from the elastic channel. Apparently, this occurs because the contributions ΔV_J and ΔW_J of the spin-density terms have no appreciable effect on the elastic

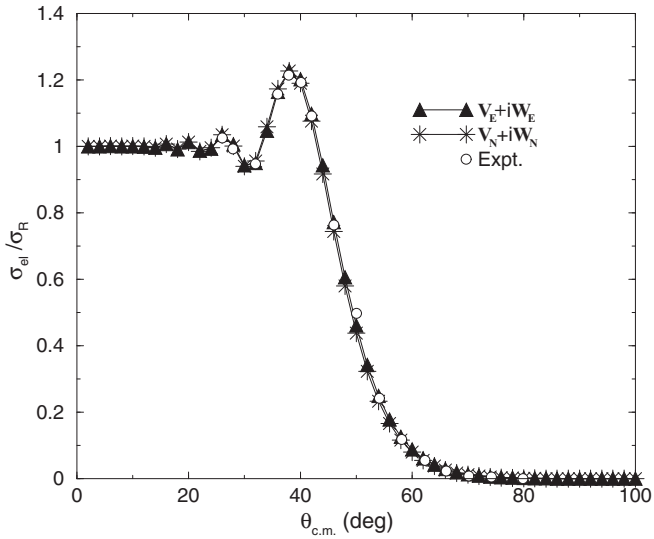

FIG. 7. Comparison of ratios of the elastic scattering cross section to Rutherford cross sections, σ_{El}/σ_R, of $^{18}\mathrm{O} + {}^{60}\mathrm{Ni}$ at $E_{\mathrm{c.m.}} = 48.46$ MeV computed from the optical potentials with the experimental data.

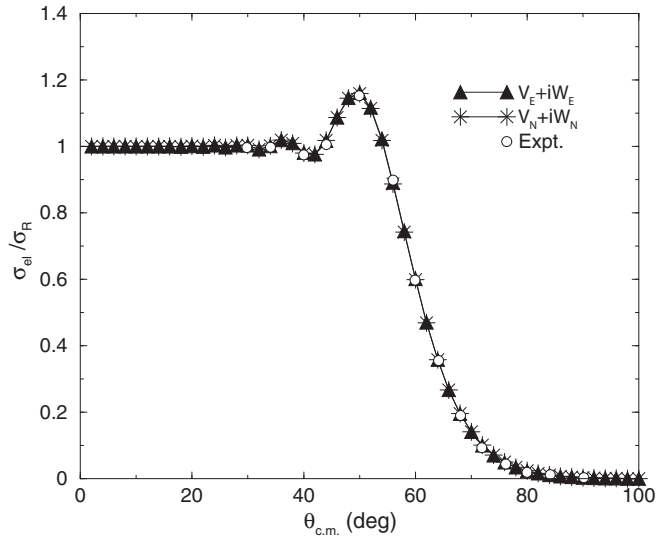

FIG. 8. Comparison of ratios of the elastic scattering cross section to Rutherford cross sections, σ_{El}/σ_R, of $^{32}\mathrm{S} + {}^{34}\mathrm{S}$ at $E_{\mathrm{c.m.}} = 49.97$ MeV computed from the optical potentials with the experimental data.

scattering cross section of spin-unsaturated open j-shell nuclei considered in the present work.

IV. SUB-BARRIER FUSION

It is evident from the analysis of elastic scattering results presented in Table IV that, when the colliding nuclei are at a distance $D < D_{1/100}$, the outgoing elastic channel is completely unpopulated. The reaction proceeds in the nonelastic channels, including fusion; i.e., before the colliding nuclei touch each other at $R_{12} < D < D_{1/100}$, they encounter the fusion barrier. As the absorption into the compound nucleus is confined to a well-defined radial region, $D_m > D > D_{1/100}$, in the reaction processes, the absorption under the barrier is not needed for explaining the sub-barrier fusion data. In other words, the sub-barrier fusion data are well described by the real part of the optical potential since the absorption becomes very insensitive to the strength and other details of the imaginary

TABLE IV. Numerical values of the scattering angles θ_m and $\theta_{1/100}$, the separation distances D_m and $D_{1/100}$, and the percentage contributions ΔV_J and ΔW_J of the spin-density terms toward the optical potential $V_E + iW_E$ at these distances.

System	$\frac{2\pi}{\lambda}$ (fm^{-1})	θ_m (deg)	D_m (fm)	$\Delta V_J(D_m)$	$\Delta W_J(D_m)$	$\theta_{1/100}$ (deg)	$D_{1/100}$ (fm)	$\Delta V_J(D_{1/100})$	$\Delta W_J(D_{1/100})$
$^{16}\mathrm{O} + {}^{20}\mathrm{Ne}$	3.64	16	13.4	0.01	1.02	55.3	7.88	2.63	2.57
$^{16}\mathrm{O} + {}^{42}\mathrm{Ca}$	4.93	30	12.88	0.02	0.84	52	8.69	0.75	0.86
$^{16}\mathrm{O} + {}^{44}\mathrm{Ca}$	4.99	30	12.73	0.02	0.57	50	8.81	1.39	1.63
$^{16}\mathrm{O} + {}^{52}\mathrm{Cr}$	5.20	36	12.76	0.01	0.23	57.3	9.3	0.7	0.9
$^{16}\mathrm{O} + {}^{54}\mathrm{Fe}$	5.25	40	11.72	0.01	0.1	63.5	8.66	1.33	1.65
$^{16}\mathrm{O} + {}^{58}\mathrm{Ni}$	5.33	42	12.99	0.02	0.18	65.5	9.77	0.54	0.71
$^{16}\mathrm{O} + {}^{62}\mathrm{Ni}$	5.41	42	12.82	0.00	0.06	65.5	9.63	0.4	0.56
$^{16}\mathrm{O} + {}^{64}\mathrm{Ni}$	5.44	40	13.18	0.01	0.09	62.6	9.83	0.26	0.34
$^{16}\mathrm{O} + {}^{74}\mathrm{Ge}$	5.41	52	13.13	0.00	0.01	79.3	10.28	0.15	0.22
$^{16}\mathrm{O} + {}^{76}\mathrm{Ge}$	5.43	52	13.09	0.01	0.03	77.5	10.35	0.22	0.31
$^{16}\mathrm{O} + {}^{92}\mathrm{Zr}$	5.80	64	13.01	0.00	0.06	94.6	10.64	0.08	0.12
$^{18}\mathrm{O} + {}^{60}\mathrm{Ni}$	5.69	38	13.55	0.12	0.78	71.5	9.02	2.48	2.76
$^{18}\mathrm{O} + {}^{62}\mathrm{Ni}$	5.73	40	12.96	0.14	0.75	73	8.95	2.45	2.74
$^{18}\mathrm{O} + {}^{64}\mathrm{Ni}$	5.77	38	13.35	0.14	0.76	69.5	9.03	1.9	2.11
$^{18}\mathrm{O} + {}^{76}\mathrm{Ge}$	5.64	52	13.35	0.18	0.69	91	9.78	1.62	1.86
$^{24}\mathrm{Mg} + {}^{32}\mathrm{S}$	6.74	18	14.90	0.06	0.61	39.7	7.95	5.35	5.87
$^{32}\mathrm{S} + {}^{34}\mathrm{S}$	6.30	18	12.42	0.41	1.12	85	9.15	2.88	3.26
$^{24}\mathrm{Mg} + {}^{36}\mathrm{S}$	7.07	50	14.19	0.07	0.76	37	7.97	3.98	4.33
$^{12}\mathrm{C} + {}^{62}\mathrm{Ni}$	4.42	34	13.29	0.17	2.91	76.6	8.86	6.01	7.1
$^{58}\mathrm{Ni} + {}^{64}\mathrm{Ni}$	12.99	52	16.10	0.06	0.33	92	11.73	1.37	1.64

TABLE V. Numerical values of the positions R_{BE} and R_{BN} and heights V_{BE} and V_{BN} of the fusion barrier and the fusion cross sections σ_{fE} and σ_{fN} calculated from the potentials V_E and V_N.

System	$E_{\text{c.m.}}$ (MeV)	R_{BE} (fm)	V_{BE} (MeV)	σ_{fE} (mb)	R_{BN} (fm)	V_{BN} (MeV)	σ_{fN} (mb)
$^{16}O + ^{20}Ne$	30.88	7.20	8.62	1170.5	7.23	8.676	1177.5
$^{16}O + ^{42}Ca$	43.45	8.13	21.46	1049.0	8.14	21.46	1051.77
$^{16}O + ^{44}Ca$	44	8.17	21.20	1087.95	8.20	21.20	1093.29
$^{16}O + ^{52}Cr$	45.88	8.49	25.47	1005.9	8.51	25.48	1010.28
$^{16}O + ^{54}Fe$	46.29	8.58	28.38	893.3	8.61	28.41	897.80
$^{16}O + ^{58}Ni$	47.03	8.85	29.68	906.2	8.87	29.68	910.15
$^{16}O + ^{62}Ni$	47.69	8.83	30.00	907.2	8.85	30.03	910.14
$^{16}O + ^{64}Ni$	48	8.88	29.32	962.9	8.90	29.36	964.95
$^{16}O + ^{74}Ge$	46.04	9.30	34.04	707.1	9.31	34.04	708.26
$^{16}O + ^{76}Ge$	46.26	9.39	33.62	755.5	9.40	33.62	757.16
$^{16}O + ^{92}Zr$	47.70	9.88	41.867	374.1	9.89	41.87	374.75
$^{18}O + ^{60}Ni$	48.46	9.02	28.37	1058.5	9.06	28.37	1067.78
$^{18}O + ^{62}Ni$	48.83	8.93	29.08	1011.9	8.96	29.09	1020.24
$^{18}O + ^{64}Ni$	49.17	9.01	28.27	1082.9	9.04	28.27	1090.19
$^{18}O + ^{76}Ge$	45.28	9.59	32.83	792.8	9.62	32.83	798.98
$^{24}Mg + ^{32}S$	68.57	7.28	14.24	1329.9	7.58	17.18	1350.23
$^{32}S + ^{34}S$	49.97	8.92	33.69	813.5	8.98	33.71	825.24
$^{24}Mg + ^{36}S$	72	7.53	13.48	1446.6	7.71	15.25	1470.42
$^{12}C + ^{62}Ni$	40.22	8.41	22.74	963.9	8.48	22.75	979.46
$^{58}Ni + ^{64}Ni$	114.99	10.42	94.73	600.7	10.47	94.75	610.9

potential. Thus, we examine here the question of to what extent the spin-density contribution affects the sub-barrier fusion data at an energy $E_{\text{c.m.}}$ where the calculated optical potential $V_E + iW_E$ reproduces the elastic scattering data of the colliding open-j shell nuclei, without any renormalization.

The heavy-ion fusion cross section σ_f, for a target-projectile spin-independent interaction, is obtained in terms of the partial-wave expansion as

$$\sigma_f = \frac{\lambda^2}{4\pi}\sum_L (2L+1)P_L, \tag{18}$$

where P_L is the transmission coefficient which describes the probability of compound nucleus formation by an incident partial wave with orbital angular momentum L. By taking the nuclear potential to be real and approximating the potential near the barrier by a parabola, one obtains P_L in the WKB approximation as

$$P_L = \left\{1 + \exp\left[2\pi(\mu/\hbar^2|V''(R_B)|)^{\frac{1}{2}}(V(R_B) - E_{\text{c.m.}})\right]\right\}^{-1}, \tag{19}$$

where

$$V(R_B) = [V_C(D) + V_N(D) + V_L(D)]|_{D=R_B}, \tag{20}$$

$$V''(R_B) = \frac{d^2}{dD^2}[V_C(D) + V_N(D) + V_L(D)]|_{D=R_B}, \tag{21}$$

and $V_C(D)$, $V_N(D)$, and $V_L(D)$ are the Coulomb, nuclear, and centrifugal potentials of the colliding nuclei. The position $D = R_B$ is calculated from the following relations:

$$[V_C(D) + V_N(D) + V_L(D)]|_{D=R_B} = E_{\text{c.m.}}, \tag{22}$$

$$\frac{d}{dD}[V_C(D) + V_N(D) + V_L(D)]|_{D=R_B} = 0, \tag{23}$$

$$\frac{d^2}{dD^2}[V_C(D) + V_N(D) + V_L(D)]|_{D=R_B} < 0. \tag{24}$$

Thus, the barrier penetration model, Eqs. (18)–(24), does not contain any free parameter except those entering through the two-body Skyrme effective interaction v_{sky}.

We have calculated the fusion barrier positions R_{BE} and R_{BN}, heights V_{BE} and V_{BN}, and fusion cross sections σ_{fE}, σ_{fN} of all the pairs of colliding open-j shell nuclei at specified energy, using the real potentials V_E and V_N in Eqs. (18)–(24). These results are presented in Table V.

Table V shows that the fusion barrier occurs 0.5 fm inside of the distance $D_{1/100}$ of complete absorption. The contribution of spin-density terms around the position R_{BE} of the fusion barrier is repulsive and enhances the values of the position R_{BE} and height V_{BE} of the fusion barrier and the fusion cross section σ_{fE} as well. Among all the pairs of colliding nuclei considered here, the percentage contribution of the spin-density terms toward V_E, R_{BE}, V_{BE}, and σ_{fE} are appreciable for the doubly spin-unsaturated colliding nuclei. In case of $^{24}Mg + ^{32}S$, at $E_{'} = 68.57$ MeV, the spin-density terms affect the potential at the fusion barrier by about 7% and the height of the fusion barrier by 21%. However, the corresponding fusion cross section is affected by only about 1.5%, since the fusion cross section is determined not only by the potential $V(R_B)$ but also by $V''(R_B)$.

V. CONCLUSION

We have calculated both the energy-dependent real V_E and imaginary W_E parts of the optical potential of some twenty

pairs of spin-unsaturated, open j-shell nuclei in the energy density model, using the complex Skyrme III energy density. These colliding nuclei have a wide range of combinations of neutron and proton spin densities arising from their n, l, and j values of the last unfilled l shell. Our systematic study on the role of spin-density terms of Skyrme III energy density reveals that the spin-density contribution toward the imaginary potential W_E is always larger than it is toward the real potential V_E. The contributions in both the real and imaginary potentials increase with greater number of valence nucleons in a fixed orbital $j = l + 1/2$ or when the valence nucleons are at higher n or l orbitals or when number of neutron and proton orbitals of the projectile and target nucleon remain unsaturated. The pairs of doubly spin-unsaturated shell nuclei make a larger spin-density contribution. Among the twenty pairs of open j-shell nuclei considered in this work, the spin-density contributions are found to be as high as 18%–19% at the repulsive maxima. However, the contribution gradually decreases to zero as the separation distance D increases beyond the maxima.

The elastic scattering cross sections of all the pairs of nuclei exhibit a Fresnel diffractive pattern of angular distributions. This type of scattering data is very much sensitive to the variation of the real and imaginary potentials [4–6]. It is found that the calculated optical potential $V_E + iW_E$, without any variation or renormalization, nicely reproduces the experimental data on elastic scattering cross sections for all pairs of nuclei studied here. The elastic scattering data are found to be sensitive to the potential $V_E + iW_E$ in a wide radial range $D_i \geqslant D \geqslant D_{1/100}$ of about 6 fm in the surface region. In this region, the contributions of the spin-density terms toward the potentials V_E and W_E are found to be up to 6% and 7%, respectively.

Next, in the barrier penetration model we have calculated the fusion barrier positions and heights and the fusion cross sections of all pairs of nuclei, using the same potential V_E. The percentage contributions of the spin-density terms toward these quantities of fusion of the colliding open j-shell nuclei are found to be larger than that of closed j-shell nuclei. The differences in the heights of the fusion barriers can be up to 21%. However, in our systematic study of the role of spin-density terms in the sub-barrier fusion, we have not taken into account the coupled-channel effects of vibrational and rotational excited states of the projectile and target nuclei, even though the experimental consequences of these effects are important [34–38].

Finally, we note that both the elastic scattering and sub-barrier fusion of all the pairs of open j-shell nuclei considered at a specific energy occur when the colliding nuclei are at a distance $D_i \geqslant D \geqslant R_{BE}$. The position R_{BE} of the fusion barrier is about 2 fm larger than the sum of their half-density radii R_{12}. In this region, the overlap density ρ is always smaller than the nuclear matter density ρ_{nm}. The maximum overlap of the densities of projectile and target nuclei among all the pairs is found to be 56% of the nuclear matter density ρ_{nm} in case of sub-barrier fusion of ^{24}Mg + ^{32}S at R_B. Such an overlap can be considered as a weak overlap and the use of the sudden approximation for the composite density ρ and the spin density $\vec{J}$ and the use of Skyrme effective interaction are valid. Therefore, the numerical values of the calculated optical potential in the radial region $D_i \geqslant D \geqslant R_B$ are qualitatively correct. In this region, although the contribution of spin-density terms are found to be appreciable toward the optical potential of several pairs of open j-shell nuclei, the exit channel events such as the Fresnel diffractive pattern of elastic scattering cross section and the sub-barrier fusion cross section are not affected much by the contribution of the spin-density terms. On the other hand, the contribution of the spin-density terms becomes very large as the separation distance D between the colliding nuclei further decreases from R_B to R_{12} and R_{12} to D_{ma}. It may, therefore, play a crucial role in determining the exit channel events such as rainbow scattering [39–45] and transfer reactions [12–15], which are sensitive to the potential in this interior region. For such an analysis, however, one has to obtain microscopically the reliable potential. This is being attempted.

ACKNOWLEDGMENTS

The authors would like to acknowledge with thanks the computational facilities provided by Dr. S. Kailas, BARC, Mumbai, India, and Dr. S. Mandal, GSI, Germany, for the calculation of the heavy-ion elastic scattering cross sections reported in this paper. This work was supported by the Department of Science and Technology, Government of India, under Grants No. SP/S2/K-23/97 and No. SP/S2/K-02/2000.

[1] S. Kaur and P. Chattopadhyay, Phys. Rev. C **36**, 1016 (1987).
[2] K. C. Panda, Phys. Rev. C **42**, 1155 (1990).
[3] K. C. Panda, J. Phys. G: Nucl. Phys. **11**, 1323 (1985).
[4] K. C. Panda and T. Patra, J. Phys. G: Nucl. Phys. **14**, 1489 (1988).
[5] K. C. Panda and T. Patra, J. Phys. G: Nucl. Part. Phys. **17**, 185 (1991).
[6] K. C. Panda and T. Patra, J. Phys. G: Nucl. Part. Phys. **16**, 593 (1990).
[7] M. Beiner, H. Flocard, N. Van Giai, and P. Quentin, Nucl. Phys. A **238**, 29 (1975).
[8] F. L. Stancu and D. M. Brink, Nucl. Phys. A **270**, 236 (1976).
[9] D. Vautherin and D. M. Brink, Phys. Rev. C **5**, 626 (1972).
[10] R. K. Puri and R. K. Gupta, J. Phys. G: Nucl. Part. Phys. **17**, 1933 (1991).
[11] R. K. Puri and R. K. Gupta, Phys. Rev. C **45**, 1837 (1992).
[12] R. K. Puri, P. Chattopadhyay, and R. K. Gupta, Phys. Rev. C **43**, 315 (1991).
[13] R. K. Puri and R. K. Gupta, Int. J. Mod. Phys. E **1**, 269 (1992).
[14] M. K. Sharma, H. Kumar, R. K. Puri, and R. K. Gupta, Phys. Rev. C **56**, 1175 (1997).
[15] R. K. Puri, R. Arora, and R. K. Gupta, Phys. Rev. C **60**, 054619 (1999).
[16] H. De Vries, C. W. De Jäger, and C. De Vries, At. Data and Nucl. Data Tables **36**, 495 (1987).

[17] L. R. B. Elton, *Nuclear Sizes* (Oxford University Press, London, 1961).
[18] P. Chattopadhyay and R. K. Gupta, Phys. Rev. C **30**, 1191 (1984).
[19] M. Hugi, L. Jarczyk, B. Kamys, J. Lang, R. Müller, E. Ungricht, and W. Zipper, J. Phys. G: Nucl. Phys. **6**, 1257 (1980); B. T. Kim, W. Y. So, S. W. Hong, and T. Udagawa, Phys. Rev. C **65**, 044616 (2002).
[20] J. W. Negele and D. Vautherin, Phys. Rev. C **5**, 1472 (1975).
[21] R. Hofstädter, Annu. Rev. Nucl. Sci. **7**, 231 (1957).
[22] A. G. Sitenko and V. K. Tartakovskii, *Lectures on the Theory of the Nucleus* (Pergamon, New York, 1975), p. 113.
[23] K. E. Rehm, W. Henning, J. R. Erskine, D. G. Kovar, M. H. Macfarlane, S. C. Pieper, and M. Rhoades-Brown, Phys. Rev. C **25**, 1915 (1982).
[24] H. H. Gutbrod, M. Blann, and W. G. Winn, Nucl. Phys. A **213**, 285 (1973).
[25] E. M. Takagui, G. R. Satchler, H. Takai, K. Koide, and O. Dietzsch, Nucl. Phys. A **514**, 120 (1990).
[26] M. C. Mermaz, Phys. Rev. C **36**, 1192 (1987).
[27] N. Goncalves, Ph.D. thesis, University of Paris, 1980.
[28] F. D. Becchetti, P. R. Christensen, V. I. Manko, and R. J. Nickles, Nucl. Phys. A **203**, 1 (1973).
[29] M. Gai, G. M. Berkowitz, P. Braun-Muzinger, C. M. Jachcinski, C. E. Ordoriez, T. R. Renner, and C. D. Uhlhorn, Phys. Rev. C **30**, 925 (1984).
[30] J. A. Ruiz, J. L. Ferrero, B. Bilwes, and R. Bilewes, Nucl. Phys. A **548**, 510 (1992).
[31] K. E. Rehm, H. J. Korner, M. Richter, H. P. Rother, J. P. Schiffer, and H. Spieler, Phys. Rev. C **12**, 1945 (1975).
[32] P. R. Christensen, I. Chernov, E. E. Gross, R. Stokstad, and F. Videbek, Nucl. Phys. A **207**, 433 (1973).
[33] K. E. Rehm, F. L. H. Wolfs, A. M. van den Berg, and W. Henning, Phys. Rev. Lett. **55**, 280 (1985).
[34] H. Esbensen and S. Landowne, Phys. Rev. C **35**, 2090 (1987).
[35] H. Esbensen, S. H. Fricke, and S. Landowne, Phys. Rev. C **40**, 2046 (1989).
[36] H. Esbensen, Phys. Rev. C **81**, 034606 (2010).
[37] J. J. Kolata *et al.*, Phys. Rev. C **85**, 054603 (2012).
[38] H. M. Jia, C. J. Lin, F. Yang, X. X. Xu, H. Q. Zhang, Z. H. Liu, L. Yang, S. T. Zhang, P. F. Bao, and L. J. Sun, Phys. Rev. C **86**, 044621 (2012).
[39] D. T. Khoa and W. von Oertzen, Phys. Lett. B **342**, 6 (1995).
[40] M. A. Candido Ribeiro, L. C. Chamon, D. Pereira, M. S. Hussein, and D. Galetti, Phys. Rev. Lett. **78**, 3270 (1997).
[41] D. T. Khoa, W. von Oertzen, H. G. Bohlen, and F. Nuoffer, Nucl. Phys. A **672**, 387 (1999).
[42] A. A. Ogloblin *et al.*, Phys. Rev. C **62**, 044601 (2000).
[43] D. T. Khoa, Phys. Rev. C **63**, 034007 (2001).
[44] S. Szilner, M. P. Nicoli, Z. Basrak, R. M. Freeman, F. Haas, A. Morsad, M. E. Brandan, and G. R. Satchler, Phys. Rev. C **64**, 064614 (2001).
[45] W. von Oertzen, H. G. Bohlen, V. Subotin, and D. T. Khoa, Acta Phys. Pol. B **33**, 93 (2002).